Journal of Materials Chemistry A

Elucidating Metal and Ligand Redox Activities of Copper-Benzoquinoid Coordination Polymer as Cathode for Lithium-Ion Batteries

Journal:	*Journal of Materials Chemistry A*
Manuscript ID	TA-COM-05-2019-005244.R1
Article Type:	Communication
Date Submitted by the Author:	20-Jul-2019
Complete List of Authors:	Chang, Cheng-Han; Tamkang University, Chemistry Li, An-Che; National Cheng Kung University, Chemical Engineering; National Cheng Kung University, Hierarchical Green-Energy Materials Research Center Popovs, Ilja; Oak Ridge National Laboratory, Chemical Sciences Division Kaveevivitchai, Watchareeya; National Cheng Kung University, Chemical Engineering; National Cheng Kung University, Hierarchical Green-Energy Materials Research Center Chen, Jeng-Lung; National Synchrotron Radiation Research Center, Chou, Kai-Chun; Tamkang University, Chemistry Kuo, Ting-Shen; National Taiwan Normal University, Chemistry Chen, Teng-Hao; Tamkang University College of Science, Chemistry

COMMUNICATION

Elucidating Metal and Ligand Redox Activities of Copper-Benzoquinoid Coordination Polymer as Cathode for Lithium-Ion Batteries

[l]Received 00th January 20xx,
Accepted 00th January 20xx

DOI: 10.1039/x0xx00000x

Cheng-Han Chang,[a,‡] An-Che Li,[bc,‡] Ilja Popovs,[d] Watchareeya Kaveevivitchai,[bc] Jeng-Lung Chen,[e] Kai-Chun Chou,[a] Ting-Shen Kuo,[f] and Teng-Hao Chen*[a]

A novel redox-active quinone-based organic building block 1,4-dicyano-2,3,5,6-tetrahydroxybenzene (LH_4) has been synthesized, and used as a bridging ligand to form a new 1D copper-benzoquinoid coordination polymer $[CuL(DMF)_2]_n$. The compound is able to deliver an initial capacity as high as 268 mAh g^{-1} at 30 mA g^{-1} (~C/2.5) when used as cathode in Li batteries. *Ex situ* XPS and FT-IR reveal the involvement of both Cu and the organic moieties in the multi-electron redox reaction. Cu K-edge XANES and EXAFS measurements confirm the change in the oxidation state and coordination environment of Cu during discharge-charge process. *In situ* generated metallic nanoparticles have been observed by TEM. The obtained mechanistic understanding of the metal-organic electrode materials for Li-based batteries may pave the way for the design of next-generation energy-storage systems.

Over the past few decades, Li-ion batteries (LIBs) have been considered one of the best energy storage technologies for small electronic devices. However, the currently emerging applications such as electric vehicles and large-scale energy storage systems, have put great demands on the next-generation LIBs.[1, 2] Higher energy density, safety, and environmental friendliness are now required at substantially lower cost. The electrode materials used in the conventional LIBs are transition-metal-based inorganic intercalation compounds and graphite as cathode and anode, respectively. Over the years, monumental efforts have been made on the transition-metal-based cathodes (layered $LiCoO_2$ in particular), such as doping, coating, and partial substitution of Co with Ni/Mn, to optimize the performance of currently commercial LIBs, and to increase the practical capacities which are much lower than their theoretical values.[3, 4] However, further enhancement of the energy density is becoming more challenging, and it appears that the inorganic materials have reached critical limits in their performance.[5]

As an alternative for transition-metal oxides, organic compounds, especially those containing carbonyls, have gained significant interest as electrode materials for rechargeable batteries. They can be designed to incorporate reversible redox-active functional groups, comprising naturally abundant elements (C, H, O, N, and S) without expensive and toxic transition metals.[5, 6] In addition to low cost and environmental friendliness, organic materials can contain a large number of redox active sites capable of undergoing a multielectron-transfer process leading to a high theoretical capacity. The redox potential of organic redox centres can be fine-tuned by introducing electron-withdrawing or electron-donating functional groups. Moreover, most organic materials can offer fast reaction kinetics and easy processing due to relatively flexible structures.[7, 8]

Despite these advantages, organic carbonyl-containing compounds usually suffer dissolution in electrolytes and low electronic conductivity. To overcome these issues, one approach is polymerization, which helps alleviate dissolution in electrolytes due to a significantly larger molecular weight.[9] However, this may result in a low theoretical capacity, because of the inevitable increase in the unit weight per electron uptake.[10] To enhance the electrochemical capacity, organic materials can be combined with metal ions or clusters. The strategy is to bridge metal ions that are capable of undergoing a redox reaction with redox-active organic bridging ligands to form coordination polymers (CPs).[11, 12] This class of materials can have different dimensionalities such as 1D chains, 2D layers, and 3D frameworks. Porous coordination polymers (PCPs) which are also known as metal-organic frameworks (MOFs) can

[a.] *Department of Chemistry, Tamkang University, Tamsui Dist., New Taipei City 25137, Taiwan. E-mail: thchen@mail.tku.edu.tw*
[b.] *Department of Chemical Engineering, National Cheng Kung University, Tainan City 70101, Taiwan*
[c.] *Hierarchical Green-Energy Materials Research Center, National Cheng Kung University, Tainan City 70101, Taiwan*
[d.] *Chemical Sciences Division, Oak Ridge National Laboratory, Oak Ridge, P.O. Box 2008, TN 37831, USA*
[e.] *National Synchrotron Radiation Research Center, Hsinchu 30076, Taiwan*
[f.] *Department of Chemistry, National Taiwan Normal University, Taipei 11677, Taiwan*
‡ These authors contributed equally to this work.
†Electronic Supplementary Information (ESI) available: Details on the synthesis and characterisation. CCDC 1914195. For ESI and crystallographic data in CIF or other electronic format See DOI: 10.1039/x0xx00000x

possess a variety of pore sizes and redox-active functionalities, and have promise to open up many application possibilities.[13, 14]

In the context of redox chemistry, redox-active metal-organic materials have been investigated for energy storage applications.[15] MOFs or PCPs are well-known for their porosity and tunability. Nevertheless, when used as battery electrodes, MOFs with large voids usually lead to a low density of redox-active sites. Their limited channels and windows may be blocked by organic solvent molecules, which often restricts Li-ion diffusion.[15] To address these issues, crystalline 1D CPs have emerged as a promising candidate for electrode materials.[16-19] The polymeric coordination chains can be linked and stabilized by weak interactions, such as hydrogen bonds, π···π stacking, or C–H···π interactions instead of strong covalent bonds.[20] As a result, these structures possess flexible space between 1D chains, which allows rapid diffusion of Li ions and gives rise to maximum practical capacities.[17] Highly crystalline electrode materials allow structural stability and redox mechanism to be studied by performing computational simulations and using diffraction technique to monitor the structural changes.[11, 16, 21] The majority of CPs used as electrode materials are formed by carboxylate ligands, which possess low redox potential and thus usually serve as anode.[16, 18, 22, 23]

Hydroquinone, a key organic building block responsible for many biological proton–electron transfer reactions, can reversibly undergo a $2e^-$, $2H^+$ transfer to give *p*-benzoquinone.[24] Hydroquinone/*p*-benzoquinone system is considered one of the most well-studied classical organic redox reactions, and has been utilized as redox centres in LIBs.[17, 25] Herein, a novel hydroquinone-based organic building block, 1,4-dicyano-2,3,5,6-tetrahydroxybenzene (LH_4, Fig. 1a), has been synthesized. This redox-active building block with two electron-withdrawing nitrile groups can allow charge delocalisation and a relatively high redox potential, which is required for cathode materials.[26-28] The solvothermal reaction between LH_4 and $Cu(NO_3)_2{\cdot}2.5H_2O$ in *N*,*N*-dimethylformamide (DMF) at 60 °C for 2 d yielded orange crystals of a new 1D CP.

The single crystal X-ray analysis reveals the 1D structure of the compound with a chemical formula of $[CuL(DMF)_2]_n$ (Fig. 1b). The symmetric molecular structure of LH_4 promotes the formation of linear metal-ligand chains. Cu(II) has an octahedral coordination geometry, and two different C–O bond distances (1.26 Å and 1.24 Å) of ligand L are recognized in the equatorial positions.[29] As shown in Fig. S8 in Electronic Supplementary Information, the Fourier-transform infrared (FT-IR) spectrum of the ligand LH_4 shows no sign of carbonyl signal, while a stretching band at 1655 cm^{-1} is assigned as C=O for the ligand in the CP (Fig. S9). This indicates that when the CP is formed, the two adjacent hydroxyl groups in LH_4 become C=O and $C–O^-$ to form a *p*-quinoid structure, with a total of two negative charges to balance Cu(II) yielding neutral 1D CP structure. The octahedral Cu(II) is capped with two DMF molecules at its axial positions. The CP 1D chains pack closely to build a layered structure without any solvent molecules in between (Fig. 1c). Surprisingly, in this structure, the nitrile groups of the ligand do not coordinate with any metal ions as commonly found in the majority of literature.[30-32] Instead, they form unusual weak supramolecular interactions via C≡N···π[33] and C≡N···H[34] bonds. The measured distances from the nitrogen atom (nitrile group) to the centroid of ligand (Fig. 1d, orange dotted line) and the hydrogen atoms of DMF molecule (Fig. 1d, green dotted lines) are 3.43 Å and 2.97–3.07 Å, respectively.

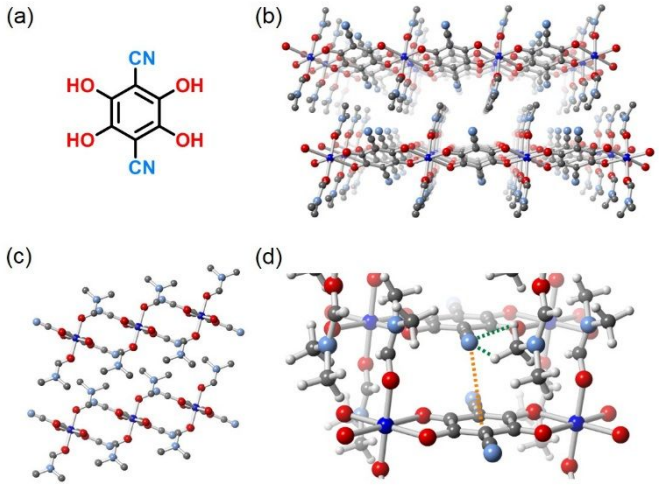

Fig. 1 (a) The chemical structure of LH_4. (b) and (c) The single crystal structure of $[CuL(DMF)_2]_n$ viewed perpendicular to and along 1D chains, respectively. The hydrogen atoms are omitted for clarity. (d) Packing of CPs by supramolecular C≡N···π (orange dotted line) and C≡N···H (green dotted lines) interactions. Colours: Cu, blue; C, grey; O, red; N, cyan; H, white.

The formation of the CP structure leads to high thermal stability as determined by thermogravimetric analysis (TGA, Fig. S11), with the loss of the coordinated DMF molecules at approximately 240 °C, followed by the decomposition at 410 °C. Powder X-ray diffraction (PXRD) analysis confirms phase purity of the 1D CP, with good agreement between the simulated and experimental patterns (Fig. S12). The interchain π–interactions provide sufficient space for Li ions, similar to π···π stacking in graphite. Additionally, when soaking the CP in various solvents, peak shifts can be observed in the PXRD patterns, suggesting structural flexibility (Fig. S13).

Despite a variety of benzoquinoid frameworks reported in the literature,[35-41] to the best of our knowledge, $[CuL(DMF)_2]_n$ is the first crystalline 1D CP based on benzoquinoid building unit to be studied as electrode for LIBs.[29, 36, 42-44] The CP was used as electrode material in coin cells (CP : Super P : KS4 : PVDF = 3:5:1:1) with Li metal as counter electrode and 1 M $LiPF_6$ in ethylene carbonate (EC)/dimethylcarbonate (DMC) (1:1) as electrolyte. Fig. 2a shows the discharge-charge profile of the CP at 30 mA g^{-1} (~C/2.5, reaction with 1 Li in 2.5 h). During discharge, a very short plateau is observed at ~2.8 V vs Li/Li^+, followed by two more plateaus at 2.35 and 1.9 V with a discharge capacity of 268 mAh g^{-1}. On charge, three plateaus can be observed at 2.15, 2.8, and 3.4 V. The positions of these plateaus are in good agreement with the cyclic voltammogram (CV) of the CP in Fig. 2b. The Cu redox couple is at 2.8/3.4 V as reported elsewhere.[11] The redox centres in the quinone-based

organic linker are responsible for the other two pairs of anodic and cathodic peaks in the CV. This shows the synergistic redox reactions on both metal centre and the organic moieties of the CP enabling multiple-electron process, which leads to a high specific capacity (with a theoretical capacity of 67 mAh g^{-1} for one electron transfer). The voltage profiles at different current densities are shown in Fig. 2c. At a higher rate, the voltages of the plateaus decrease due to kinetic effects. At 120 mA g^{-1} (~1.8C), the CP delivered an initial capacity of 213 mAh g^{-1}. Fig. 2d shows the capacity retention at different rates. At 80 mA g^{-1}, the capacity drops initially before stabilizing at 120 mAh g^{-1}.

Fig. 2 (a) Discharge-charge profile of the CP $[CuL(DMF)_2]_n$ (1st

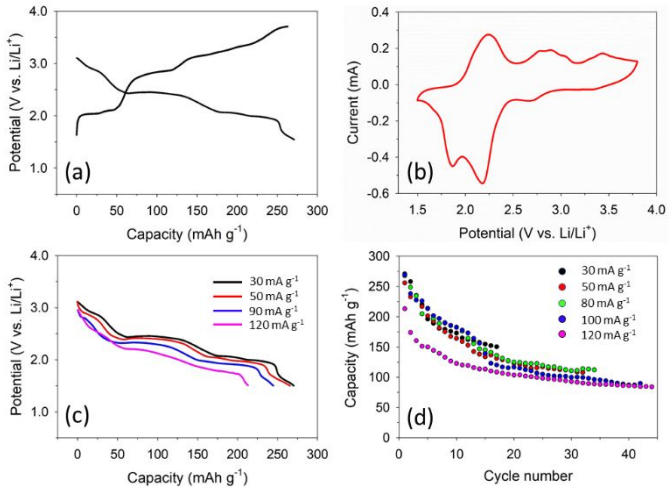

cycle) at 30 mA g^{-1} (~C/2.5) with 1 M $LiPF_6$ in EC/DMC (1:1) as electrolyte. (b) Solid-state CV of the CP with a scan rate of 0.5 mV s^{-1}. (c) Discharge curves at different current densities. (d) Capacity retention ranging from 30 mA g^{-1} (~C/2.5) to 120 mA g^{-1} (~1.8C).

Dissolution tests were performed in order to compare the stability of the CP to that of the organic ligand in electrolyte. Electrodes with the CP $[CuL(DMF)_2]_n$ and organic linker LH_4 as active materials were soaked in electrolyte for up to 5 d (Fig. S14). It was found that the CP with the 1D coordination chain was stable in the electrolyte, while the organic linker dissolved almost immediately and the colour of the electrolyte became yellowish. The electrochemical properties of LH_4 were also investigated in comparison with the CP (Fig. S15 and S16). During the first discharge, there are short plateaus at ~2.4 and 1.9 V which are very close to the plateau positions in the CP voltage profile, corresponding to the redox centres in the quinone-based organic linker. However, the capacities dropped rapidly to ~30 mAh g^{-1} within 15 cycles due to the dissolution of the organic ligand in the electrolyte. When compared to the performance of the CP electrodes, this confirms that the CP formation helps with material stability in the electrolyte.

To elucidate the change in the oxidation state of Cu(II) during discharge-charge cycle, X-ray photoelectron spectroscopy (XPS) was carried out on the CP electrodes. Fig. 3 exhibits the deconvolution of high-resolution Cu 2p spectra of electrodes at two different positions on the first cycle (at 2.5 V on discharge and 3.6 V on charge). The spectra reveal that on discharge to 2.5 V, Cu(0) and Cu(I) are present with the majority being Cu(0). Cu $2p_{3/2}$ and Cu $2p_{1/2}$ were observed at 933.5 and 953.5 eV for Cu(I) and at 932.7 and 952.46 eV for Cu(0), respectively.[19, 45, 46] The absence of Cu $2p_{3/2}$ satellite peaks at ~942 eV indicates that there is no Cu(II) remaining at 2.5 V. Subsequently, on charge to 3.6 V, the amount of Cu(0) significantly decreases with Cu(I) being the main component. This result confirms the reduction and oxidation of Cu species during discharge and charge, respectively. The deconvolution of C 1s XPS spectra does not only support the change in the metal oxidation state, but also reveals the redox process of the organic moieties. The peaks at 284.4, 285.1, and 286.4 eV are attributed to the characteristic peaks of C–C, C–O, and C=O bonds.[47] Comparing the C 1s spectra (Fig. 3, Bottom) at 2.5 V and 3.6 V, it is evident that at 2.5 V higher proportion of C–O bonds is observed than at 3.6, while it is the opposite for C=O. A change in the relative quantity between C–O and C=O at the two positions suggests the transformation of carbonyl group into enol structure during discharge confirming electron-uptake process of the organic moieties, and enol structure converting back to carbonyl during charge. From the FT-IR spectra (Fig. S19), the relative intensity of the carbonyl group at 1668 cm^{-1} decreases during discharge and becomes stronger during charge, which is in good agreement with the C 1s XPS data.[47]

Fig. 3 Deconvolution of high-resolution XPS spectra of

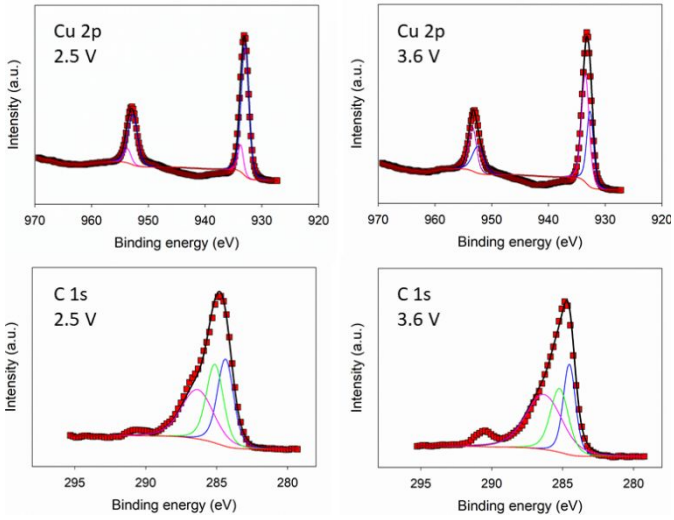

electrodes at 2.5 V on discharge and 3.6 V on charge: (Top) Cu $2p_{3/2}$ and $2p_{1/2}$ (blue: Cu(0); pink: Cu(I)). (Bottom) C 1s (blue: C–C; green: C–O; pink: C=O); 291 eV assigned to π–π* satellite peak.[47]

To further investigate the valence state change and the local structure of Cu during discharge-charge (Fig. 4a), *ex situ* Cu K-edge X-ray absorption spectroscopy (XAS) measurements were performed on the CP electrodes (CP : Super P : KS4 : PVDF = 5:3:1:1). Starting with a pristine electrode, the spectrum from X-ray absorption near edge structure (XANES) analysis (Fig. 4b) clearly shows the existence of Cu(II) species.[11] When the cell was discharged down to 2.1 V, the appearance of a pre-edge peak at 8982 eV and an edge peak shift to a lower energy show the reduction of Cu(II) species.[11, 22] Fig. 4c exhibits Cu K-edge extended X-ray absorption fine structure (EXAFS) patterns. It

can be clearly observed that the intensity of Cu–O bond became weaker, whereas Cu–Cu bond became stronger during discharge-charge, when compared to pristine material. The curve fitting (Fig. S23) of the EXAFS patterns provides a Cu–O coordination number of 3.05 per Cu in the pristine CP electrode, 1.45 for the electrode at 2.1 V on discharge, 1.12 for 1.5 V (end of discharge), and back to 1.18 for 3.2 V on charge, suggesting Cu–O bond dissociation during discharge and Cu–O bond formation during charge. This result also further supports the change in oxidation state of Cu species. High-resolution transmission electron microscopy (HR-TEM) was also conducted on the CP electrodes. As shown in Fig. 5, as the CP was discharged to 2.5 V, metallic nanoparticles of copper were found to slightly aggregate in the organic matrix with the size of ~5 nm. The interplanar spacing of 0.21 nm in Fig. 5b can be ascribed to the (111) plane of Cu metal.[47] On charge to 3.6 V, some Cu(0) is still visible in the HR-TEM images (Fig. 5c and 5d).

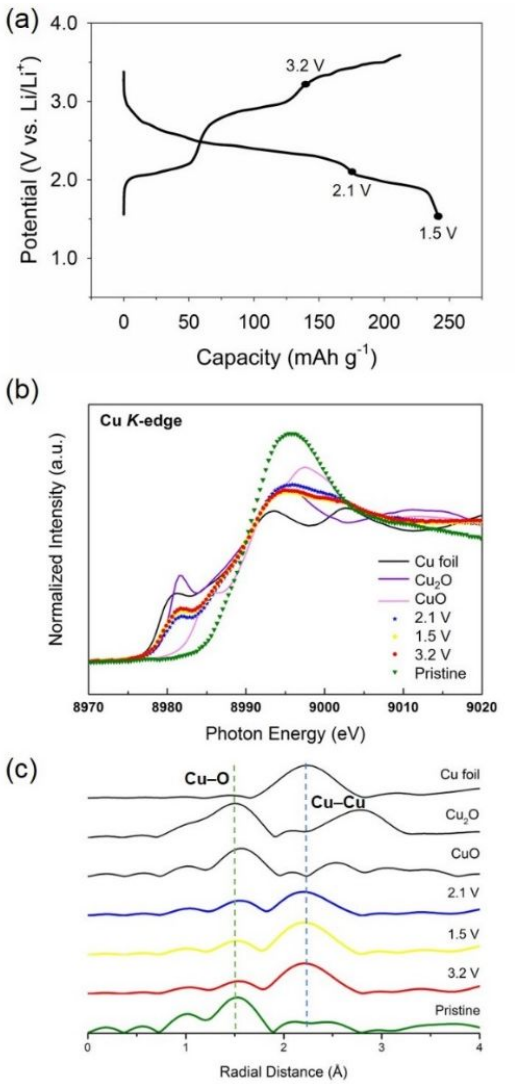

Fig. 4 (a) Voltage profile of the CP electrodes at 20 mA g^{-1}. (b) Cu K-edge XANES patterns and (c) Cu K-edge EXAFS patterns of the CP electrodes by synchrotron-sourced XAS analyses (with Cu foil, Cu_2O, and CuO as references).

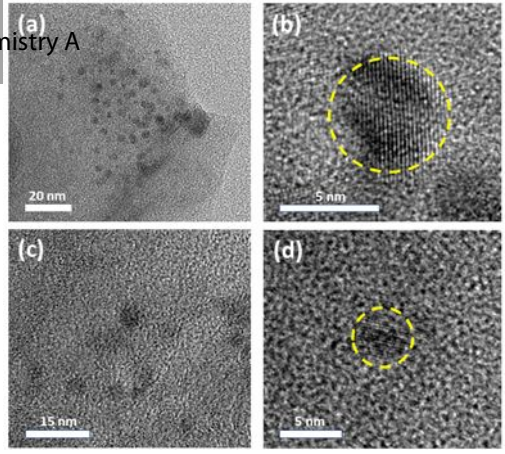

Fig. 5 HR-TEM images of CP electrodes (a, b) at 2.5 V on discharge and (c, d) at 3.6 V on charge.

Conclusions

A new quinone-based organic ligand LH_4 has been synthesized, and used to prepare 1D CP $[CuL(DMF)_2]_n$. The synergistic redox reactions on both Cu and organic moieties have been demonstrated to enable multiple-electron redox processes, leading to a high specific capacity. Cu K-edge XANES and EXAFS as well as HR-TEM have revealed the nature of Cu species during discharge-charge process. In combination with XPS and FT-IR, the ligand redox activities have also been elucidated. Without channel-size restrictions commonly encountered in 3D frameworks, the chain-based supramolecular structure of $[CuL(DMF)_2]_n$ is flexible and can accommodate volume change, which could help with Li-ion diffusion during cycling. Although the CP could deliver high initial capacity, it suffered a capacity loss. This suggests insufficient oxidation of Cu species during charge and partial extraction of Li ions, possibly due to low electronic conductivity of the CP. The obtained mechanistic understanding of the CP as electrode material for Li-based batteries could pave the way for the design of other metal-organic materials for next-generation high-performance rechargeable batteries. Furthermore, by introducing additional aromatic π···π interactions into the structure of CP, such as replacing the coordinating DMF molecule with pyridine, the electronic conductivity of the CP could potentially be enhanced, thus allowing superior electrochemical performance. This intriguing concept is currently under investigation in our laboratory and will be reported in due course.

Conflicts of interest

There are no conflicts to declare.

Acknowledgements

We acknowledge the financial support from Ministry of Science and Technology of Taiwan under grant MOST107-2113-M-032-007 (to T.-H. C.) and the Young Scholar Fellowship Program MOST108-2636-E-006-001 (to W. K.). Research by I. P. was supported by U.S. Department of Energy, Office of Science, Basic Energy Sciences, Materials Sciences and Engineering Division.

Notes and references

1. S. Lee, G. Kwon, K. Ku, K. Yoon, S.-K. Jung, H.-D. Lim and K. Kang, *Adv. Mater.*, 2018, **30**, 1704682.
2. A. Mauger and C. M. Julien, *Ionics*, 2017, **23**, 1933–1947.
3. A. Manthiram, *J. Phys. Chem. Lett.*, 2011, **2**, 176–184.
4. W. Kaveevivitchai and A. J. Jacobson, *Chem. Mater.*, 2013, **25**, 2708–2715.
5. B. Häupler, A. Wild and U. S. Schubert, *Adv. Energy Mater.*, 2015, **5**, 1402034.
6. Q. Zhao, Z. Zhu and J. Chen, *Adv. Mater.*, 2017, **29**, 1607007.
7. M. E. Bhosale, S. Chae, J. M. Kim and J.-Y. Choi, *J. Mater. Chem. A*, 2018, **6**, 19885–19911.
8. K. C. Kim, *Ind Eng Chem Res*, 2017, **56**, 12009–12023.
9. Z. Song, Y. Qian, X. Liu, T. Zhang, Y. Zhu, H. Yu, M. Otani and H. Zhou, *Energy Environ. Sci.*, 2014, **7**, 4077–4086.
10. J. Xie, P. Gu and Q. Zhang, *ACS Energy Lett.*, 2017, **2**, 1985–1996.
11. Z. Zhang, H. Yoshikawa and K. Awaga, *J. Am. Chem. Soc.*, 2014, **136**, 16112–16115.
12. Z. Zhang, H. Yoshikawa and K. Awaga, *Chem. Mater.*, 2016, **28**, 1298–1303.
13. Z. Zhang and K. Awaga, *MRS Bulletin*, 2016, **41**, 883–889.
14. Z. Liang, C. Qu, W. Guo, R. Zou and Q. Xu, *Adv. Mater.*, 2018, **30**, 1702891.
15. Z. Wu, J. Xie, Z. J. Xu, S. Zhang and Q. Zhang, *J. Mater. Chem. A*, 2019, **7**, 4259–4290.
16. L. Zhang, F. Cheng, W. Shi, J. Chen and P. Cheng, *ACS Appl. Mater. Interfaces*, 2018, **10**, 6398–6406.
17. J. Xiang, C. Chang, M. Li, S. Wu, L. Yuan and J. Sun, *Cryst. Growth Des.*, 2008, **8**, 280–282.
18. G. Li, H. Yang, F. Li, F. Cheng, W. Shi, J. Chen and P. Cheng, *Inorg. Chem.*, 2016, **55**, 4935–4940.
19. S. M. D. Watson, N. G. Wright, B. R. Horrocks and A. Houlton, *Langmuir*, 2010, **26**, 2068–2075.
20. L. Sieuw, A. Jouhara, É. Quarez, C. Auger, J.-F. Gohy, P. Poizot and A. Vlad, *Chem. Sci.*, 2019, **10**, 418–426.
21. W. Kaveevivitchai and A. Manthiram, *J. Mater. Chem. A*, 2016, **4**, 18737–18741.
22. H. H. Lee, J. B. Lee, Y. Park, K. H. Park, M. S. Okyay, D.-S. Shin, S. Kim, J. Park, N. Park, B.-K. An, Y. S. Jung, H.-W. Lee, K. T. Lee and S. Y. Hong, *ACS Appl. Mater. Interfaces*, 2018, **10**, 22110–22118.
23. Y. Song, L. Yu, Y. Gao, C. Shi, M. Cheng, X. Wang, H.-J. Liu and Q. Liu, *Inorg. Chem.*, 2017, **56**, 11603–11609.
24. M. Rafiee and D. Nematollahi, *Electroanalysis*, 2007, **19**, 1382–1386.
25. W. Kaveevivitchai, X. Wang, L. Liu and A. J. Jacobson, *Inorg. Chem.*, 2015, **54**, 1822–1828.
26. Y. Hanyu, Y. Ganbe and I. Honma, *J. Power Sources*, 2013, **221**, 186–190.
27. T. Liu, M.-M. Liu, X.-W. Zheng, C.-Y. Du, X.-Y. Cui, L. Wang, L.-L. Han and Z.-Y. Yu, *Tetrahedron*, 2014, **70**, 9033–9040.
28. K. Sato, H. Imai and Y. Oaki, *ACS Appl. Nano Mater.*, 2018, **1**, 4218–4226.
29. S. Kawata, S. Kitagawa, H. Kumagai, C. Kudo, H. Kamesaki, T. Ishiyama, R. Suzuki, M. Kondo and M. Katada, *Inorg. Chem.*, 1996, **35**, 4449–4461.
30. M. Munakata, G. L. Ning, T. Kuroda-Sowa, M. Maekawa, Y. Suenaga and T. Horino, *Inorg. Chem.*, 1998, **37**, 5651–5656.
31. T. Kuroda-Sowa, T. Horino, M. Yamamoto, Y. Ohno, M. Maekawa and M. Munakata, *Inorg. Chem.*, 1997, **36**, 6382–6389.
32. M. K. Broderick, C. Yang, R. D. Pike, A. Nicholas, D. May and H. H. Patterson, *Polyhedron*, 2016, **114**, 333–343.
33. F. Setifi, D. K. Geiger, I. Abdul Razak and Z. Setifi, *Acta Cryst.*, 2015, **71**, 658–663.
34. A. Peter, M. Mohan, T. Maris, J. D. Wuest and A. Duong, *Cryst. Growth Des.*, 2017, **17**, 5242–5248.
35. T.-T. Luo, Y.-H. Liu, H.-L. Tsai, C.-C. Su, C.-H. Ueng and K.-L. Lu, *Eur. J. Inorg. Chem.*, 2004, **2004**, 4253–4258.
36. B. F. Abrahams, T. A. Hudson, L. J. McCormick and R. Robson, *Cryst. Growth Des.*, 2011, **11**, 2717–2720.
37. L. E. Darago, M. L. Aubrey, C. J. Yu, M. I. Gonzalez and J. R. Long, *J. Am. Chem. Soc.*, 2015, **137**, 15703–15711.
38. J. A. DeGayner, I.-R. Jeon, L. Sun, M. Dincă and T. D. Harris, *J. Am. Chem. Soc.*, 2017, **139**, 4175–4184.
39. I.-R. Jeon, B. Negru, R. P. Van Duyne and T. D. Harris, *J. Am. Chem. Soc.*, 2015, **137**, 15699–15702.
40. L. Liu, J. A. DeGayner, L. Sun, D. Z. Zee and T. D. Harris, *Chem. Sci.*, 2019, **10**, 4652–4661.
41. L. Liu, L. Li, J. A. DeGayner, P. H. Winegar, Y. Fang and T. D. Harris, *J. Am. Chem. Soc.*, 2018, **140**, 11444–11453.
42. J. A. DeGayner, K. Wang and T. D. Harris, *J. Am. Chem. Soc.*, 2018, **140**, 6550–6553.
43. S. Kawata, S. Kitagawa, M. Kondo and M. Katada, *Synthetic Metals*, 1995, **71**, 1917–1918.
44. H. Kumagai, S. Kawata and S. Kitagawa, *Inorganica Chim. Acta*, 2002, **337**, 387–392.
45. X. Wang, B. Zhang, W. Zhang, M. Yu, L. Cui, X. Cao and J. Liu, *Sci. Rep.*, 2017, **7**, 1584.
46. Z. Jin, C. Liu, K. Qi and X. Cui, *Sci. Rep.*, 2017, **7**, 39695.
47. J. Wang, Q. Deng, M. Li, K. Jiang, J. Zhang, Z. Hu and J. Chu, *Sci. Rep.*, 2017, **7**, 8903.

Novel 1D copper-benzoquinoid coordination polymer with both metal and ligand redox activities gives a capacity as high as 240 mAh g^{-1}.

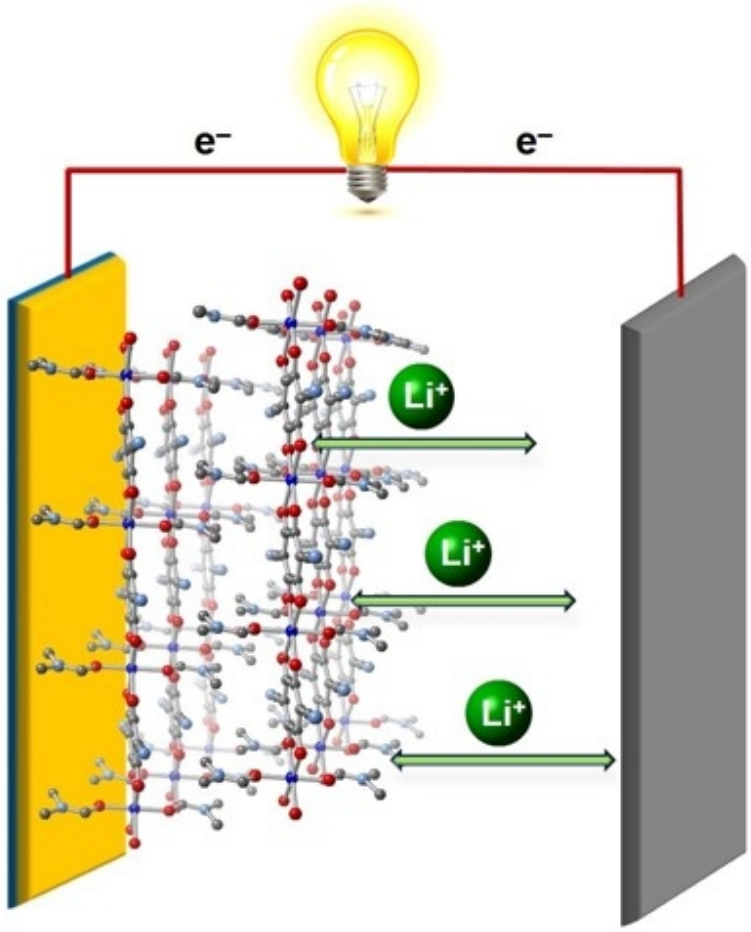

86x99mm (150 x 150 DPI)